Advanced Wetland Mapping with GEE and Sentinel Imagery: A Tool for Conservation of the Sidi Moussa Oualidia Complex

Marwa ZERROUK[1], Kenza AIT EL KADI[1], Imane SEBARI[1], Siham FELLAHI[1]
[1] Institut Agronomique et Vétérinaire Hassan II, Morocco

Keywords: Wetlands, Mapping, Google Earth Engine, Multi-sensor, Machine Learning, Sidi Moussa Oualidia.

Abstract

Wetlands are considered among the most productive ecosystems on Earth, as they shelter a diversity of species and maintain ecological balance. However, their ongoing degradation threatens biodiversity and ecosystems, underscoring the need for regular and long-term monitoring. The Sidi Moussa Oualidia wetland complex, a Ramsar site in Morocco, is a critical habitat for migratory birds and an invaluable ecological resource known for its complex landscape patterns. In this study, we present a framework in Google Earth Engine (GEE) that fuses optical, radar, texture, and terrain data with both pixel- and object-based classification to map and classify wetlands at 10 m resolution. We first generate a cloud-free Sentinel-2 composite using Scene Classification masking and pansharpen the 20 m SWIR band (B11) to 10 m, enabling precise computation of NDWI, MNDWI, and GLCM texture indices. A Sentinel-1 VV/VH ratio and SRTM-derived slope are added to the stack. A pixel-level Random Forest (RF) classifier is trained on stratified samples to produce an initial map. We then segment the RGB composite into superpixels via Simple Non-Iterative Clustering (SNIC) and assign each superpixel its majority RF class, smoothing speckle and salt-and-pepper noise while preserving ecologically meaningful object boundaries. Validation against ground truth points yields an overall accuracy of 94 % and a Kappa of 0.91—an 8 % improvement over pixel-only results. Our first-of-its-kind approach in Morocco, designed to capture the complex spatial patterns of heterogeneous wetland environments, provides a promising solution for operational wetland monitoring and supports informed spatial decision-making in water resource management and ecological conservation.

1. Introduction

Wetlands are considered valuable resources and among the most productive ecosystems, as they provide essential ecological services such as water purification, flood mitigation, and carbon sequestration (X. Xu et al. 2020). They also shelter several species and play a crucial role in maintaining the ecological balance (Aslam, Naz, et al. 2024). Beyond their environmental roles, wetlands serve as critical habitats for a variety of species, particularly migratory birds, amphibians, and endemic plants (Kumari, Das, and Kumar 2023). Despite their ecological significance, wetlands worldwide face severe degradation due to anthropogenic pressures, including urban expansion, agricultural encroachment, pollution, and climate change (T. Xu et al. 2019). This degradation threatens not only biodiversity but also regional ecological stability and socio-economic wellbeing.

The Sidi Moussa Oualidia wetland complex, located along the Atlantic coast of Morocco and designated as a Ramsar site, reflects this ecological importance. It forms a vital node along the East Atlantic Flyway and serves as a seasonal refuge for thousands of migratory birds (El Hamoumi et al. 2022). Its mosaic of coastal lagoons, salt marshes, mudflats, and surrounding semi-arid zones makes it both ecologically unique and complex to monitor (El Hamoumi et al. 2022). However, like many wetlands globally, this area is under increasing threat from land-use change, overexploitation of natural resources, and hydrological alterations (Mahrad et al. 2022). The lack of consistent, up-to-date, and spatially explicit information hampers effective conservation and adaptive management efforts in the region.

In this context, remote sensing technologies have emerged as vital tools for large-scale and long-term wetland monitoring. Specifically, medium-resolution satellite imagery, such as that from Sentinel-2, offers an open-access solution for capturing multi-temporal and multispectral observations of wetland dynamics (Aslam, Shu, et al. 2024) (Ghorbanian et al. 2021). Coupled with powerful cloud-based platforms such as Google Earth Engine (GEE), researchers can now process, analyze, and visualize massive datasets rapidly, overcoming the computational limitations of local processing (Tamiminia et al. 2020).

Traditional wetland mapping has relied heavily on spectral indices like the Normalized Difference Water Index (NDWI) and Modified NDWI (MNDWI) derived from optical satellite imagery (Ashok, Rani, and Jayakumar 2021) (Kaplan and Avdan 2017). However, these approaches are often limited by cloud cover, lack of temporal sensitivity, and reduced accuracy in transitional or mixed land cover zones. In addition, few methods integrate key features such as seasonal dynamics, textural complexity, and terrain elevation which are crucial for identifying heterogeneous wetland environments (Aslam, Shu, et al. 2024).

In this paper, we develop a framework to map the Sidi Moussa Oualidia wetland complex using Sentinel-2 and Sentinel-1 data within Google Earth Engine. We begin by detailing the preprocessing steps and the construction of a multi-dimensional feature stack incorporating spectral, temporal, SAR, texture, and topographic variables. We then describe the classification process, which combines pixel-based Random Forest modelling with object-based smoothing through a super-pixel non-iterative clustering (SNIC) segmentation. The results section evaluates the accuracy of the classification using performance metrics. Finally, we discuss the implications of the findings for wetland monitoring and conservation, and we conclude with recommendations for future applications.

[1] Institut Agronomique et Vétérinaire Hassan II, Rabat, Maroc

2. Study Area and Methodology

2.1 Study Area

The study was conducted over the Sidi Moussa Oualidia wetland complex, located between the village of Sidi El Abed in the north (33°02'49''N), 35 km south of El Jadida, and the town of Oualidia in the south (32°44'03''N), 66 km north of Safi (El Hamoumi et al. 2022). This site, listed under the Ramsar Convention, is composed of shallow lagoons, tidal mudflats, and seasonal salt marshes. The region is subject to a Mediterranean semi-arid climate with pronounced wet and dry seasons, making it ideal for testing temporally sensitive classification workflows (El Hamoumi et al. 2022) (figure 1).

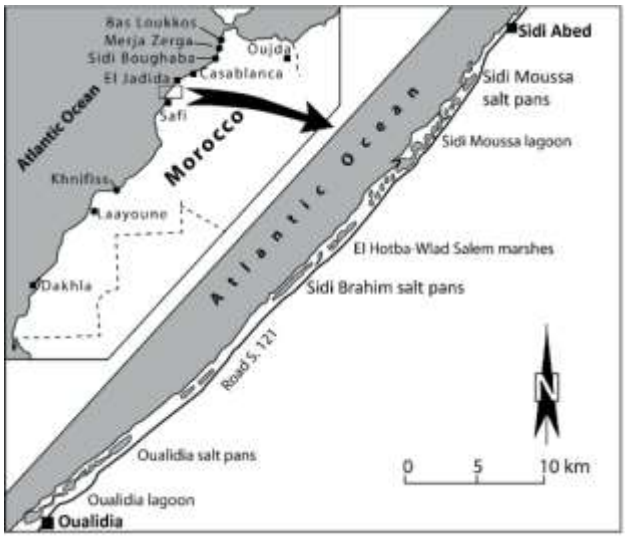

Figure 1: Location of The Sidi Moussa Oualidia Complex (El Hamoumi et al. 2022)

2.2 Methodology

To monitor and map the spatial characteristics of the wetland, we used satellite imagery acquired from the Sentinel-2 and Sentinel-1 platforms within the Google Earth Engine (GEE) environment. Sentinel-2 provides optical imagery through 13 spectral bands in the visible, near-infrared (NIR), and short-wave infrared (SWIR) regions. The spatial resolution varies from 10 m to 60 m, depending on the band. Sentinel-2 Level-2A Surface Reflectance data from the year 2018 were used, focusing on two distinct seasonal windows: wet season (February–April) and dry season (July–October)(C. Zhao et al. 2023).

Additionally, radar data from Sentinel-1 (GRD, dual-polarization VV and VH) were incorporated to overcome cloud limitations and detect inundation through backscatter properties. The Sentinel-1 mission, also part of the Copernicus Program, provides consistent SAR data at 10-meter resolution with a revisit frequency of 6 days. Terrain elevation data were derived from the SRTM DEM (30 m resolution), enabling topographic context to be added to the classification model (Minotti et al. 2021).

Figure 2 explicates the workflow that was adopted in our paper below.

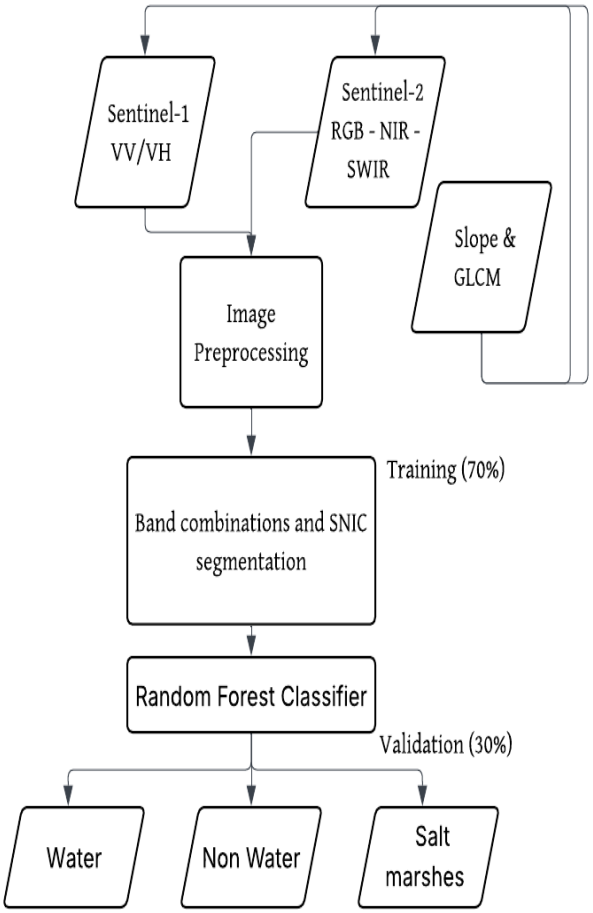

Figure 2: Workflow for Multi-sensor Feature Stacking, SNIC Segmentation, and Random-Forest Classification in GEE

2.2.1 Preprocessing

- **Sentinel-2 Image Preparation:**

Sentinel-2 Level-2A imagery for the year 2018 was filtered using a cloud coverage threshold of <20%. To ensure the quality of surface reflectance data, a custom cloud and shadow mask was applied based on the Scene Classification Layer (SCL). Pixels marked as cloud, cirrus, shadow, or saturated were excluded.

Two seasonal composites were generated:

- Wet Season Composite: February to April 2018
- Dry Season Composite: July to October 2018

Each composite was created using the median pixel value across the selected time range to reduce noise and capture consistent seasonal signatures.

- **Pansharpening SWIR (B11)**

To improve the spatial resolution of the SWIR band used in MNDWI calculation, we implemented a pansharpening technique using a synthetic panchromatic image derived from the mean of high-resolution visible bands (B2, B3, B4). The SWIR band (originally at 20m) was resampled to 10m and enhanced by adding the high-frequency details extracted from

the panchromatic proxy using a Gaussian convolution kernel. This step enabled more spatially precise detection of water boundaries, particularly in fragmented salt marsh zones such as the ones in the Sidi Moussa Oualidia Complex (Sahour, Kemink, and O'connell 2022).

From the pre-processed imagery, we constructed a multi-dimensional feature stack combining spectral, temporal, topographic, and radar-based information:

- **NDWI (Normalized Difference Water Index)**

Computed using green (B3) and near-infrared (B8) bands to emphasize open water surfaces, as they reflect green light and absorb NIR.

$$NDWI = \frac{B3 - B8}{B3 + B8}$$

- **MNDWI (Modified NDWI)**

Incorporates SWIR instead of NIR, making it more effective in urbanized or vegetated wetland zones.

$$MNDWI = \frac{B3 - B11(ps)}{B3 + B11(ps)}$$

Where B11(ps) = the pansharpened SWIR band.

- **NDWI Amplitude**

Calculated as the difference between NDWI values in wet and dry seasons to represent seasonal water variability. It is a strong indicator of ephemeral wetlands and flooded salt marshes.

$$NDWI\_amp = NDWI(wet) - NDWI(dry)$$

- **Gray-Level Co-occurrence Matrix Texture (GLCM)**

A texture metric derived from the NDWI image using a 3×3 Gray-Level Co-Occurrence Matrix (GLCM). The contrast band quantifies local spatial heterogeneity, especially useful in saltmarsh zones, where mixed vegetation and soil produce unique textural patterns (Adeli et al. 2022).

- **Slope**

Derived from the SRTM DEM to introduce topographic context. Wetlands typically occupy low-lying flat areas, and slope helps distinguish between water accumulation zones and adjacent elevated terrain (Peng et al. 2023).

- **VV/VH Ratio (SAR Feature)**

From Sentinel-1, the VV/VH polarization ratio was used to highlight flooded vegetation, soil moisture variations, and areas with different surface roughness. SAR is especially useful in wetlands where water is partially obscured by vegetation or cloud cover is frequent (Koutsos et al. 2025).

2.2.3 Classification Approach

Training Data and Random Forest Classifier:

Training samples were manually annotated over high-resolution maps in Google Earth, representing three land cover classes:

- Non-water (label 0)
- Water (label 1)
- Saltmarsh (label 2)

A Random Forest (RF) classifier was trained using 100 decision trees and the full feature stack. The data were split into 70% training and 30% validation, with random stratified sampling to ensure balanced class representation. The RF model was chosen for its robustness to overfitting and ability to handle multi-dimensional features.

Object-Based Segmentation with SNIC:

Simple Non-Iterative Clustering (SNIC) was used in GEE to apply a Superpixel-based segmentation following the pixel-based classification (Shafizadeh-Moghadam et al. 2021). SNIC creates spatially coherent segments (superpixels) based on spectral similarity and proximity. It was applied to the RGB composite (bands B4, B3, B2), resampled at 30 meters and using the parameters set shown in Table 1. This produced a "clusters" raster in which each superpixel shares a unique label ID. Lastly, we used a mode reducer to combine the SNIC labels and the per-pixel Random Forest predictions in a "reduceConnectedComponents" method, which allowed us to reassign each segment its majority class. The result is an object-based classification raster in which every superpixel has been uniformly labelled according to its dominant RF class, yielding smoother boundaries and more ecologically coherent objects.

Parameter	Value
Size	15
compactness	1
connectivity	8
neighborhoodSize	64
Seeds	auto-generated

Table 1: Configuration of SNIC segmentation parameters for superpixel-based smoothing in post-classification analysis

Accuracy assessment:

The accuracy assessment has been made for both our pixel- and object-based maps, using the same held-out validation points to ensure a fair comparison. First, we randomly split our ground-truth sample points 70/30 into training and validation sets. After running each classifier, we used Earth Engine's sampleRegions (with a small tileScale and an unmask(–1) step) to extract predicted labels at each validation location. We then extracted our confusion matrix and derived the necessary metrics from it.

3. Results

3.1 Pixel-based Random Forest Classifier

The pixel-based RF results indicate generally strong performance, but with some systematic biases worth noting. The confusion matrix shows that out of 18 true non-water pixels, 17 were correctly labeled, while one was misclassified as saltmarsh. 24 of 28 pixels for water were correctly identified, with three confused as non-water and one as saltmarsh. Saltmarsh proved slightly confusing: 25 of 29 pixels were labeled correctly, but three were mapped as non-water and one as water (figure 3).

The model achieves an 88 % accuracy and a Cohen's Kappa of 0.82. When we look at the recall, the RF correctly retrieves 94 % of true non-water areas, but only about 86 % of both water and saltmarsh pixels. This implies that approximately 14% of

actual water pixels are not detected, even though non-water pixels are rarely overlooked.
On the other hand, precision reveals that when the model does predict water or saltmarsh, it is almost always correct—96 % precision for water and 92.6 % for saltmarsh. Non-water predictions, however, contain more false alarms: only about 74 % of pixels labeled non-water are truly terrestrial, the remainder being misclassified wetlands. The harmonic mean of precision and recall (the F_1-score) follows this pattern: 0.91 for water, 0.89 for saltmarsh, but 0.83 for non-water.

Finally, class imbalance likely affects these rates: there are over 300 000 non-water pixels and 250 000 water pixels in the test set, but only about 52 000 saltmarsh pixels. The relative scarcity of saltmarsh means fewer training examples and a greater chance of omission. Overall, the pixel-RF baseline is robust—especially for open water—but tends to over-predict non-water at the expense of water classes, indicating room for improvement via object-based smoothing.
Table 2 summarizes per-class performance metrics of the RF-classifier.

Class	Recall	Precision	F_1-Score
Non-wetland (0)	94.4 %	73.9 %	0.83
Water (1)	85.7 %	96.0 %	0.91
Saltmarsh (2)	86.2 %	92.6 %	0.89

Table 2: Performance metrics of the Pixel-based RF classifier

Figure 3: Pixel-based Random Forest classification of a subsection of the Sidi Moussa Oualidia lagoon (blue = open water, green = saltmarsh, gray = non-water)

3.2 Object-based RF Classifier

The object-based classification delivers very strong and coherent results across all three classes, outperforming the pixel-based approach (Figure 4). In terms of overall agreement, it correctly labels 93.94 % of the validation samples, with a Cohen's Kappa of 0.91. This high Kappa reflects that most of the improvement comes from reducing misclassifications rather than simply capitalizing on class imbalances.

A closer look at the confusion matrix reveals where these gains occur. For the non-water class, 32 out of 34 samples (94 %) are correctly identified, with only two misclassified as saltmarsh. Water achieves 89 % recall (16 of 18 samples), with one sample each mislabeled as non-water and saltmarsh. Crucially, saltmarsh reaches perfect recall—14 of 14 samples—meaning no true saltmarsh pixels are omitted. These numbers show that object-based smoothing virtually eliminates the random "salt-and-pepper" errors that often plague pixel-by-pixel maps, especially in heterogeneous wetlands (Table 3).

Precision and F_1-scores further confirm this robustness. When the model predicts water, it is correct 100 % of the time (no commission errors), and non-water predictions are 97 % accurate. Saltmarsh predictions, while perfectly sensitive, include some false positives (precision = 82 %), suggesting that a few non-marsh pixels fall within marsh-dominated superpixels. Nevertheless, all classes achieve F_1-scores above 0.90—0.955 for non-water, 0.941 for water, and 0.903 for saltmarsh—indicating an excellent balance between recall and precision (Table 4).

Compared to the pixel-based Random Forest (which achieved 88 % overall accuracy and Kappa = 0.82), the SNIC-RF workflow raises overall accuracy by nearly 6 points and Kappa by 0.08. It eliminates all omissions of saltmarsh pixels and boosts water precision from 96 % to 100 %. These improvements demonstrate that object-based segmentation followed by a simple mode aggregation effectively enforces spatial consistency, reduces speckle, and produces a more thematically coherent wetland map—essential attributes for reliable, operational monitoring of complex coastal ecosystems.

True ↓ \ Pred →	Non-water (0)	Water (1)	Saltmarsh (2)
Non-water	32	0	2
Water	1	16	1
Saltmarsh	0	0	14

Table 3: Confusion Matrix of the object-based classification

Figure 4: Object-based Random Forest classification of a subsection of the Sidi Moussa Oualidia lagoon (Blue = open water, green = saltmarsh, Grey = non-water)

Class	Recall	Precision	F_1-Score
Non-water (0)	94.1 %	97.0 %	0.955
Water (1)	88.9 %	100 %	0.941
Saltmarsh (2)	100 %	82.4 %	0.903

Table 4: Performance metrics of the Object-based RF classifier

4. Discussion

Our object-based SNIC–RF workflow (OA = 93.9%, Kappa = 0.90) substantially outperforms the pixel-level RF baseline (OA = 88%, Kappa = 0.82), confirming the value of superpixel smoothing and multi-source feature stacking in wetland classification. Similar SNIC–RF couplings in other contexts have consistently yielded 1–6 % gains in overall accuracy and notable Kappa improvements. For instance, (Ke et al. 2024) applied SNIC–RF with feature selection and sample migration over China's Liaohe Estuary and observed OA increases of 0.69–5.82 % and Kappa gains up to 0.0751 compared to pure RF approaches .

In agricultural mapping, (Khamnoi, Homhuan, and Suwanprasit 2024) fused Sentinel-1 VV/VH and Sentinel-2 bands into an SNIC–RF scheme, achieving OA = 97% and Kappa = 0.94—closely mirroring our object-level performance despite different landscapes and classes. Likewise, in Turkey's Sakarbasi wetlands, (Kaplan and Avdan 2017) showed that combining object segmentation with NDVI/NDWI index-based refinements on Sentinel-2 imagery, delivered a Kappa of 0.95, illustrating how superpixel boundaries guided by spectral indices sharpen wetland delineation.

(KARAKUŞ 2024)'s object-based analysis of Lake Köyceğiz, integrating SNIC with RF and SVM, reported water-area F_1-scores > 0.98 and OA > 92% across four years—again highlighting SNIC's role in reducing "salt & pepper" noise and elevating class purity. (Tassi and Vizzari 2020) similarly demonstrated that augmenting SNIC with GLCM-derived texture and RF on Sentinel-2 boosted OA from 82% (pixel RF) to 89.3% (object RF) . Our 93.9 % OA thus represents a further step forward, owing in part to our richer feature stack (NDWI, MNDWI, seasonal amplitude, GLCM contrast, slope, VV/VH ratio).

In the Great Lakes region itself, (Mohseni et al. 2023) used an object-based RF within GEE to distinguish Bog, Fen, Marsh, and Swamp, attaining OA = 87% and Kappa = 0.91.
By comparison, our workflow's multi-sensor fusion and mode-based superpixel classification push accuracy to 93.9% and Kappa = 0.91, underscoring the importance of stacking complementary optical, SAR, and textural predictors.

Crucially, our approach remains memory-safe and computationally lightweight, even over large Ramsar-scale areas, because superpixel generation reduces the data volume for classification and avoids unbounded image operations. While methods like sample migration and wrapper-based feature selection can further refine object-level training, our results demonstrate that a well-tuned SNIC segmentation plus a robust RF on a multi-dimensional stack already yields state-of-the-art wetland mapping—efficiently and at high resolution.

5. Perspectives and Recommendations

Although our SNIC–RF workflow delivers strong single-year wetland maps, wetlands change continuously through seasons and across years (Mao et al. 2025). Extending the pipeline to produce annual or even seasonal maps would reveal how water levels, vegetation cover, and salt marsh extents fluctuate over time. Incorporating a leave-one-year-out validation scheme would test whether our model trained on one season or year still accurately predicts in another, highlighting its robustness to changing conditions (Allgaier and Pryss 2024).

Our current feature stack combines optical, radar, texture, and terrain layers, but feeding all of these into the classifier can introduce redundancy and increase processing time. Future work should explore automated feature-selection techniques to pare down to the most informative bands and indices. Likewise, once stable training samples have been identified, "sample migration" methods could carry those reference points forward in time, reducing the need to redraw field samples each season and keeping ground-truth efforts to a minimum (Ke et al. 2024).

While SNIC superpixels give us uniform, memory-safe segments that smooth out speckle noise, modern deep-learning approaches—like U-Net convolutional networks—learn fine object boundaries directly from imagery without preset segmentation rules and are capable of identifying complex patterns of wetlands (Jamali et al. 2022).

SNIC is just one choice among many superpixel or graph-based clustering methods. It would be valuable to benchmark clustering methods (J. Zhao, Xiong, and Zhu 2024).

To understand how widely our framework applies, we should deploy it on other wetland sites—whether other Ramsar sites along the coast, inland lakes, or river floodplains. Running the same workflow elsewhere will help reveal how differences in terrain slope, vegetation type, or water regimes influence classification quality and may point to automated rules for choosing optimal parameters.

Finally, the real power of a cloud-based, memory-safe system lies in real-time or near-real-time monitoring. By scheduling

periodic runs in GEE, we could generate automatic alerts when the wetland extent shrinks suddenly or when flooding persists longer than usual. Linking those outputs to hydrodynamic or weather models would put early-warning tools into the hands of managers. Above all, future work must bridge our classification maps with on-the-ground ecological surveys, water-quality sampling, and ecosystem-service assessments, so that the maps directly inform conservation strategies and water-resource decisions.

References

Adeli, S., L. J. Quackenbush, B. Salehi, and M. Mahdianpari. 2022. "The Importance of Seasonal Textural Features for Object-Based Classification of Wetlands: New York State Case Study." International Archives of the Photogrammetry, Remote Sensing and Spatial Information Sciences - ISPRS Archives 43 (B3-2022): 471–77. https://doi.org/10.5194/isprs-archives-XLIII-B3-2022-471-2022.

Allgaier, Johannes, and Rüdiger Pryss. 2024. "Cross-Validation Visualized: A Narrative Guide to Advanced Methods." Machine Learning and Knowledge Extraction 6 (2): 1378–88. https://doi.org/10.3390/make6020065.

Ashok, Amgoth, Hari Ponnamma Rani, and K. V. Jayakumar. 2021. "Monitoring of Dynamic Wetland Changes Using NDVI and NDWI Based Landsat Imagery." Remote Sensing Applications: Society and Environment 23 (May): 100547. https://doi.org/10.1016/j.rsase.2021.100547.

Aslam, Rana Waqar, Iram Naz, Hong Shu, Jianguo Yan, Abdul Quddoos, Aqil Tariq, J. Brian Davis, Adel M. Al-Saif, and Walid Soufan. 2024. "Multi-Temporal Image Analysis of Wetland Dynamics Using Machine Learning Algorithms." Journal of Environmental Management 371 (June): 123123. https://doi.org/10.1016/j.jenvman.2024.123123.

Aslam, Rana Waqar, Hong Shu, Kanwal Javid, Shazia Pervaiz, Farhan Mustafa, Danish Raza, Bilal Ahmed, Abdul Quddoos, Saad Al-Ahmadi, and Wesam Atef Hatamleh. 2024. "Wetland Identification through Remote Sensing: Insights into Wetness, Greenness, Turbidity, Temperature, and Changing Landscapes." Big Data Research 35 (November 2023): 100416. https://doi.org/10.1016/j.bdr.2023.100416.

Ghorbanian, Arsalan, Soheil Zaghian, Reza Mohammadi Asiyabi, Meisam Amani, Ali Mohammadzadeh, and Sadegh Jamali. 2021. "Mangrove Ecosystem Mapping Using Sentinel-1 and Sentinel-2 Satellite Images and Random Forest Algorithm in Google Earth Engine." Remote Sensing 13 (13): 1–18. https://doi.org/10.3390/rs13132565.

Hamoumi, Rhimou El, Siham El Malki, Abdeslam Rihane, Abdelhak Fahmi, and Mohamed Dakki. 2022. "The Sidi Moussa-Oualidia Wetland Complex: A Bird Paradise between Land and Sea." Frontiers in Science and Engineering 12 (1). https://doi.org/10.34874/IMIST.PRSM/fsejournal-v12i1.31633.

Jamali, Ali, Masoud Mahdianpari, Brian Brisco, Dehua Mao, Bahram Salehi, and Fariba Mohammadimanesh. 2022. "3DUNetGSFormer: A Deep Learning Pipeline for Complex Wetland Mapping Using Generative Adversarial Networks and Swin Transformer." Ecological Informatics 72 (July): 101904. https://doi.org/10.1016/j.ecoinf.2022.101904.

Kaplan, G., and U. Avdan. 2017. "MAPPING and MONITORING WETLANDS USING SENTINEL-2 SATELLITE IMAGERY." ISPRS Annals of the Photogrammetry, Remote Sensing and Spatial Information Sciences 4 (4W4): 271–77. https://doi.org/10.5194/isprs-annals-IV-4-W4-271-2017.

KARAKUŞ, Pınar. 2024. "Object Based Classification in Google Earth Engine Combining SNIC and Machine Learning Methods (Case Study: Lake Köyceğiz)." Turkish Journal of Remote Sensing and GIS 5 (March): 125–37. https://doi.org/10.48123/rsgis.1411380.

Ke, Lina, Qin Tan, Yao Lu, Quanming Wang, Guangshuai Zhang, Yu Zhao, and Lei Wang. 2024. "Classification and Spatio-Temporal Evolution Analysis of Coastal Wetlands in the Liaohe Estuary from 1985 to 2023: Based on Feature Selection and Sample Migration Methods." Frontiers in Forests and Global Change 7 (August): 1–15. https://doi.org/10.3389/ffgc.2024.1406473.

Khamnoi, W, S Homhuan, and C Suwanprasit. 2024. "Most Suitable SNIC Parameters and Classifier Algorithm for Object-Based Most Suitable SNIC Parameters and Classifier Algorithm for Object-Based Classification of Rice Crop Area Using Remote Sensing Images in Google Earth," no. March 2025. https://doi.org/10.53989/bu.ga.v13i2.57.

Koutsos, Thomas M, Anthoula Papachristaki, Georgios Ovakoglou, and Thomas K Alexandridis. 2025. "Surface Water Mapping in Rice Paddies and Wetlands Using SENTINEL-1 Data , Random Forests , and Texture Features" 19 (2): 1–21. https://doi.org/10.1117/1.JRS.19.021005.

Kumari, Khushbu, Bijay Kumar Das, and Sumit Kumar. 2023. "Migratory Birds in the Wetlands of Bihar: A Review Article," no. April. https://doi.org/10.13140/RG.2.2.13917.28645.

Mahrad, Badr el, Rajae Ait Ali, Mohamed Ben-Daoud, Nezha Mejjad, Meryem Touzani, and Ismail Mohsine. 2022. "A Decision Support Framework for the Management of Sidi Moussa-Oualidia Lagoons: Moving toward Sustainability" 12 (1): 111–17.

Mao, Dehua, Ming Wang, Yeqiao Wang, Ming Jiang, Wenping Yuan, Ling Luo, Kaidong Feng, et al. 2025. "The Trajectory of Wetland Change in China between 1980 and 2020: Hidden Losses and Restoration Effects." Science Bulletin 70 (4): 587–96. https://doi.org/10.1016/j.scib.2024.12.016.

Minotti, Priscilla Gail, Mariela Rajngewerc, Vanesa Alí Santoro, and Rafael Grimson. 2021. "Evaluation of SAR C-Band Interferometric Coherence Time-Series for Coastal Wetland Hydropattern Mapping." Journal of South American Earth Sciences 106 (June 2020): 102976. https://doi.org/10.1016/j.jsames.2020.102976.

Mohseni, Farzane, Meisam Amani, Pegah Mohammadpour, Mohammad Kakooei, Shuanggen Jin, and Armin Moghimi. 2023. "Wetland Mapping in Great Lakes Using Sentinel-1/2 Time-Series Imagery and DEM Data in Google Earth Engine." Remote Sensing 15 (14). https://doi.org/10.3390/rs15143495.

Peng, Kaifeng, Weiguo Jiang, Peng Hou, Zhifeng Wu, Ziyan Ling, Xiaoya Wang, Zhenguo Niu, and Dehua Mao. 2023. "Continental-Scale Wetland Mapping: A Novel Algorithm for Detailed Wetland Types Classification Based on Time Series Sentinel-1/2 Images." Ecological Indicators 148 (March): 110113. https://doi.org/10.1016/j.ecolind.2023.110113.

Sahour, Hossein, Kaylan M. Kemink, and Jessica O'connell. 2022. "Integrating Sar and Optical Remote Sensing for Conservation-Targeted Wetlands Mapping." Remote Sensing 14 (1). https://doi.org/10.3390/rs14010159.

Shafizadeh-Moghadam, Hossein, Morteza Khazaei, Seyed Kazem Alavipanah, and Qihao Weng. 2021. "Google Earth Engine for Large-Scale Land Use and Land Cover Mapping: An Object-Based Classification Approach Using Spectral, Textural and Topographical Factors." GIScience and Remote Sensing 58 (6): 914–28. https://doi.org/10.1080/15481603.2021.1947623.

Tamiminia, Haifa, Bahram Salehi, Masoud Mahdianpari, Lindi Quackenbush, Sarina Adeli, and Brian Brisco. 2020. "Google Earth Engine for Geo-Big Data Applications: A Meta-Analysis and Systematic Review." ISPRS Journal of Photogrammetry and Remote Sensing 164 (March): 152–70. https://doi.org/10.1016/j.isprsjprs.2020.04.001.

Tassi, Andrea, and Marco Vizzari. 2020. "Object-Oriented Lulc Classification in Google Earth Engine Combining Snic, Glcm, and Machine Learning Algorithms." Remote Sensing 12 (22): 1–17. https://doi.org/10.3390/rs12223776.

Xu, Ting, Baisha Weng, Denghua Yan, Kun Wang, Xiangnan Li, Wuxia Bi, Meng Li, Xiangjun Cheng, and Yinxue Liu. 2019. "Wetlands of International Importance: Status, Threats, and Future Protection." International Journal of Environmental Research and Public Health 16 (10). https://doi.org/10.3390/ijerph16101818.

Xu, Xibao, Minkun Chen, Guishan Yang, Bo Jiang, and Ji Zhang. 2020. "Wetland Ecosystem Services Research: A Critical Review." Global Ecology and Conservation 22: e01027. https://doi.org/10.1016/j.gecco.2020.e01027.

Zhao, Chuanpeng, Mingming Jia, Zongming Wang, Dehua Mao, and Yeqiao Wang. 2023. "Identifying Mangroves through Knowledge Extracted from Trained Random Forest Models: An Interpretable Mangrove Mapping Approach (IMMA)." ISPRS Journal of Photogrammetry and Remote Sensing 201 (June): 209–25. https://doi.org/10.1016/j.isprsjprs.2023.05.025.

Zhao, Jie, Zhitong Xiong, and Xiao Xiang Zhu. 2024. "UrbanSARFloods: Sentinel-1 SLC-Based Benchmark Dataset for Urban and Open-Area Flood Mapping," 419–29. https://doi.org/10.1109/CVPRW63382.2024.00047.